Finite-Difference Seismic Modeling of Discrete Fractures in a San Juan Basin Gas Reservoir

T.M. Daley, K.T. Nihei, L.R. Myer, E.L. Majer
Lawrence Berkeley National Laboratory

J.H. Queen, M. Fortuna, J. Murphy
Conoco, Inc

R.T. Coates
Schlumberger-Doll Research

For more information,
contact: Tom Daley (tmdaley@lbl.gov)
www-esd.lbl.gov/ER/projects/fracquant.html

1. Background

As part of a Dept. of Energy sponsored program in fractured gas production, we are conducting numerical modeling of seismic wave propagation in fractured media (Majer, et al., 2001). We are using the San Juan Basin in Northwest New Mexico as a focus area and investigating the seismic detection of fracturing which may control gas production. Surface seismic data, acquired and reprocessed by Conoco, is being analyzed for fracture-induced effects beginning with equivalent media based P-wave analysis. Our numerical modeling is focused on a different approach. We are studying the seismic effects of discrete fractures (or fractures zones) set in an isotropic background rather than using equivalent anisotropic media approximations. Numerical modeling of discrete fractures will be used to guide analysis of surface and borehole seismic acquisition.

2. Finite-difference Modeling

The finite-difference code uses a standard 2D staggered-grid, velocity-stress, anisotropic algorithm. The fractures are modeled as finite length columns of single grid points with equal normal and tangential stiffness. For a given fracture stiffness in a given background, the anisotropic elastic constants are defined and the wavefield is modeled using the method of Coates and Schoenberg (1995).

3. Fracture Stiffness Assignment

An important component of this work is developing an understanding of field scale fracture properties. The stiffness (or compliance) of a discrete fracture is poorly understood in field conditions. We developed a conceptual model based on lab scale observations (Fig 1). This conceptual model was used to calculate the stiffness of the short, stiff fractures in our basic model. The longer, more compliant fractures (joints) were arbitrarily assigned a stiffness 1/10 of the calculated value.

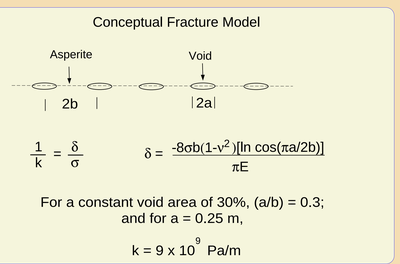

Figure 1. The calculation of fracture stiffness used in F-D modeling begins with Lab scale estimates of void length being 30% of the fracture length and a void length of 0.25 m. Assuming a constant far-field applied stress (σ), the fracture stiffness (k), associated with additional displacement (δ) is calculated from the crack geometry (a and b),along with the Young's modulus (E) and Poisson's ratio (ν) of the host material (Myer, 2000).

4. Basic Model (5 Layers, 2 Fracture Sets)

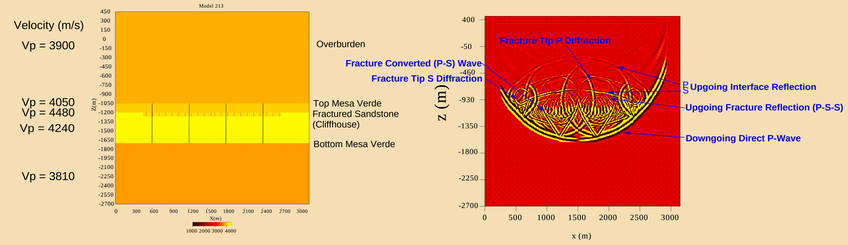

Figure 2 A simple five layer model of the San Juan Basin was developed with focus on the Mesa Verde Unit. The model has 4 through-going, low-stiffness joints, 650 m long at 600 m spacing in the Mesa Verde, and 107 bed-truncated, 60 m long, high-stiffness fractures at 21 m spacing in the Cliffhouse sandstone. The model has 1050x1050 grid points at 3 m spacing (including a 150 grid point absorbing boundary).

Figure 3 Wavefield snapshot at 400 ms time for the horizontal component of velocity for a shot at 50 m depth. Note the strong scattering and complex wavefield. While the fracture tip diffractions may not be realistic for field scale joints, the P-to-S conversions ("V" shapes) should be observable. While most energy is downgoing, surface observations (section 5) will include upgoing fracture scattered events which are reflected from the velocity interfaces.

5. Various Studies Using Shot Gathers in Basic Model

No Fractures vs Both Fracture Sets

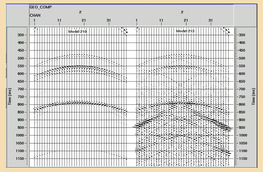

Figure 4 Comparison of the basic model with no fractures (left) and both fracture sets (right). Many coherent events are generated by the discrete fractures. Traces are the vertical component at true relative amplitude. Note that most of the additional fracture scattered energy is following the reflection for the interface below the fractures (the base of the Mesa Verde at about 800 ms).

Large Fractures/Joints Only

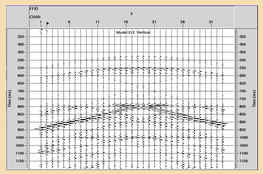

Figure 5 Vertical component shot gather for the basic model with large fractures (joints) only. Coherent events can be compared to Figure 4 (both fracture sets) to see that the dominant energy is scattered from the 4 discrete fractures with lower stiffness. Traces are true relative amplitude.

Small Fractures Only

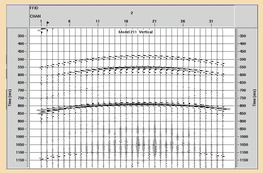

Figure 6 Vertical component shot gather (standard acquisition) for basic model with small fractures only. Instead of the coherent events seen from the large fractures in Fig. 5, "ringing" arrivals from multiple scattering are observed. Traces are true relative amplitude.

P vs S; Divergence and Curl

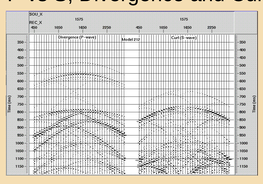

Figure 7 Shot gather for basic model with only large fractures (joints) separted into P-wave energy (divergence, left) and S-wave energy (curl, right). Traces are true relative amplitude.

Attenuation Study

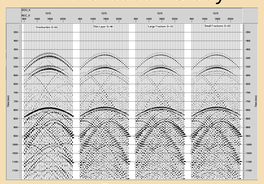

Figure 8 Shot gathers of divergence (P-waves) over the basic model with various model elements given attenuation:
A) The overburden has Q=50
B) The thin fractured sandstone layer has Q=40; C) The large fractures have an internal Q=10;
D) The small fractures have Q=25.
All these cases still contain significant energy scattered from fractures. Traces are individually normalized because of low amplitudes in A. Examples B, C and D have approximately equivalent amplitudes.

Variable Stiffness Study

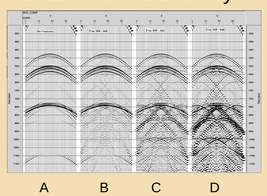

Figure 9 Shot gathers of vertical component over the basic model with only large fractures; A) No fractures; B) Fracture stiffness = $8x10^9$; C) Fractures stiffness = $3x10^9$; D) Fracture stiffness = $8x10^8$. Allowing for the lack of noise in this numerical model, this study appears to delineate the range of fracture stiffness detectable with surface methods. Traces are true relative amplitude.

Note: All shot gathers used a 50 Hz Ricker wavelet and 37 receivers at 60 m spacing. The divergence, curl and attenuation data used a vertical point source, while the other data sets had an explosive source.

6. Realistic Model (41 Layers, 1 Fracture Cluster) with CMP Data

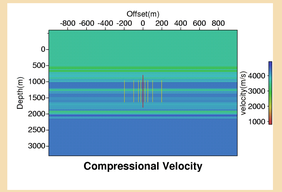

Figure 10. P-wave velocity structure for part of a realistic 6x3 km model of the San Juan basin. This 41 layer model is based on blocked well logs from the basin. One fracture "cluster" with a long, central, compliant fracture and shorter, stiffer fractures on either side is shown in this close-up. The fractures are placed in the Mesa Verde Unit.

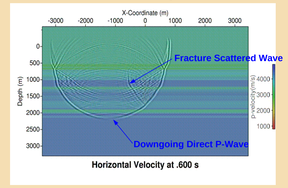

Figure 11 A snapshot of the x-component wavefield at 0.6 s for an explosive type source. The source is at X= -1200 m Note the strong back scattering from the fracture cluster.

Shot Gathers

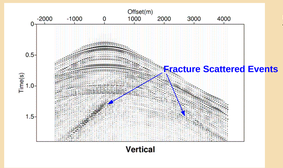

Figure 12 Vertical component shot gather for the model shown in Figure 10. Note that events with non-hyperbolic moveout are fracture scattered events. These fracture scattered events can still be detected within the complex reflectivity of a 41 layer model.

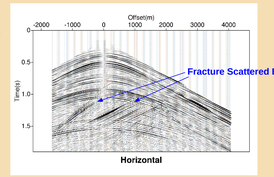

Figure 13 Horizontal component shot gather for the model shown in Figure 10. Note that events with non-hyperbolic moveout are fracture scattered events. The fracture scattered events can still be detected within the complex reflectivity of a 41 layer model. The horizontal component contains more scattered energy than the vertical.

CMP Gather

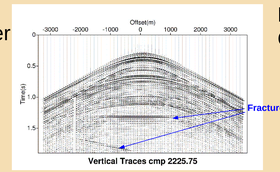

Figure 12 Vertical component, common midpoint (CMP) gather. Over one hundred shot gathers were computed to generate this cmp image. Again note that the non-hyperbolic events are fracture generated.
.

NMO Corrected CMP Gather

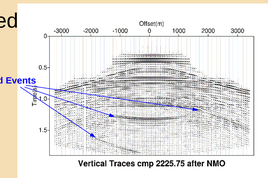

Figure 13 Vertical component, common midpoint (CMP) gather of data from Figure 12 with normal moveout (NMO) correction. In this NMO corrected data, horizontal events are the velocity interfaces, while curving or dipping events are fracture scattered events. *In "standard" processing, the fracture scattered events would be intentionally removed or attenuated to "improve" the CMP stack.*

7. Discrete Fracture Imaging

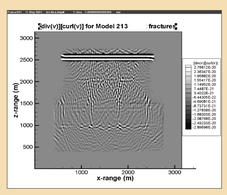

Figure 16 Because of the strong P-to-S converstions observed in the modeling, a divergence-curl imaging method was tested. The approach is an adaptation of reverse-time migration. The wavefield recorded at the receiver array is used for back propagation of the scattered curl wavefield. Concurrently, the divergence wavefield from the source is forward propagated into the medium. An image of the scatterers is formed by multiplying source-divergence and receiver-curl wavefields at each time step and adding images obtained at earlier time steps to form a composite image (Nihei, et al., 2001).

8. Conclusions

1) A realistic scale numerical model shows that energy scattered from discrete fractures or joints can be detected as coherent events in surface seismic data.
2) Fracture tip diffractions and P-to-S conversions appear to be the dominant events.
3) The stiffness of the fractures is a crucial parameter for detectability, while spatial scale and spacing are also important.
4) Standard CMP processing will not correctly image these events, instead they will be attenuated because of non-hyperbolic moveout.We are investigating imaging methods using P-to-S conversions.

References

Coates, R. T., and Schoenberg, M., Finite-difference modeling of faults and fractures, Geophysics, 60, n5,1995.
Majer, E.L., T.M. Daley, L.R. Myer, K. Nihei, J. Queen, J. Sinton, J. Murphy, M. Fortuna, H.B. Lynn, M.A. Imhoff, R. Wilson, San Juan Fracture Characterization Project: Status and Current Results, LBNL-48908, Lawrence Berkeley National Laboratory Report, 2001.
Myer, L.R., Fractures as collections of cracks, International Journal of Rock Mechanics and Mining Sciences, 37, p231, 2000.
Nihei, K.T., S. Nakagawa and L.R. Myer, Fracture imaging with converted elastic waves, Proc. of the US Rock Mech. Symp., Washington D.C., 2001.

Acknowledgements: This work was supported by the assistant Secretary for Fossil Energy, National Energy Technology Laboratory (NETL). LBNL processing was performed at the Center for Computaional Seismology, supported by the Director, Office of Science, Office of Basic Energy Sciences, Division of Engineering and Geosciences, of the U.S. Department of Energy under Contract No. DE-AC03-76SF00098. We would like to thank NETL project managers Thomas Mroz and Frances Toro for their support.

A-Z Index
Search
Phone Book

DISCLAIMER

This document was prepared as an account of work sponsored by the United States Government. While this document is believed to contain correct information, neither the United States Government nor any agency thereof, nor The Regents of the University of California, nor any of their employees, makes any warranty, express or implied, or assumes any legal responsibility for the accuracy, completeness, or usefulness of any information, apparatus, product, or process disclosed, or represents that its use would not infringe privately owned rights. Reference herein to any specific commercial product, process, or service by its trade name, trademark, manufacturer, or otherwise, does not necessarily constitute or imply its endorsement, recommendation, or favoring by the United States Government or any agency thereof, or The Regents of the University of California. The views and opinions of authors expressed herein do not necessarily state or reflect those of the United States Government or any agency thereof, or The Regents of the University of California.

Ernest Orlando Lawrence Berkeley National Laboratory is an equal opportunity employer.

Ernest Orlando Lawrence Berkeley National Laboratory

Last modified Friday, 23-Jun-00 11:06:00